

Dark Matter data and constraints on quartic couplings in IDM

Dorota Sokołowska

University of Warsaw, Faculty of Physics, Warsaw, Poland

December 7, 2018

Abstract

We analyse the thermal evolution of the Universe in the Inert Doublet Model for three regions of Dark Matter masses: low mass (4–8) GeV, medium mass (30–80) GeV and high mass (500–1000) GeV. Those three regions of DM mass exhibit different behaviour, both in the possible types of evolution and in the energy relic density values. In this analysis we use the masses of the scalar particles as the input parameters to constrain the two self-couplings between neutral scalars: λ_{345}, λ_2 . These couplings are used to construct the parameter space where different types of evolution may be presented. We discuss the influence of the scalar masses on the type of the evolution. We also discuss the importance of the λ_2 self-coupling. We argue, that the astrophysical data along with the positivity constraints simultaneously constrain both λ_{345} and λ_2 self-couplings.

1 Introduction

Inert Doublet Model (IDM) is one of the widely discussed extensions of the Standard Model (SM) that may provide the Dark Matter (DM) candidate [1, 2]. It is a Z_2 symmetric 2HDM with a suitable set of parameters. In this model two scalar doublets are introduced. Φ_S is the Higgs doublet responsible for the electroweak symmetry breaking and masses of fermions and gauge bosons as in the SM. This doublet provides the longitudinal degrees of freedom of the gauge bosons and the SM-like Higgs boson particle h_S . The other doublet, Φ_D , does not receive vacuum expectation value (v.e.v.) and does not couple to fermions. All components of this doublet are realized as the massive scalar D -particles: two charged D^\pm and two neutral D_H and D_A . The stability of the lightest of these particles, which is a candidate for the DM particle, originates from the discrete symmetry of Z_2 type, called below D -symmetry:

$$D : \quad \Phi_S \xrightarrow{D} \Phi_S, \quad \Phi_D \xrightarrow{D} -\Phi_D, \quad \text{SM fields} \xrightarrow{D} \text{SM fields}. \quad (1)$$

We assume that the current vacuum state of the Universe is described by IDM with the DM candidate D_H , so that:

$$M_{D^\pm}, M_{D_A} > M_{D_H}. \quad (2)$$

In this paper we discuss the evolution of the Universe after inflation, following the approach presented in [3, 4, 5, 6, 7]. In this approach the scalar potential changes due to the temperature corrections $\sim T^2$ and in the past, for $T \neq 0$, the vacuum structure could have different properties than the present vacuum state at $T = 0$. Sequences of the different vacua (represented on the phase diagrams by *rays*) describe different types of evolution of the Universe.

We consider the possible rays that can be realized in three regions of the DM mass: low mass (4 – 8) GeV, medium mass (30 – 80) GeV and high mass (500 – 1000) GeV. We use the estimation of the energy relic density of DM to show that for different mass regions different types of evolution are consistent with the WMAP constraints for the energy relic density of DM, $\Omega_{DM}h^2$.

In [6, 7] we focused on (μ_1, μ_2) phase diagram defined by the quadratic and two quartic parameters of the scalar potential $V_{12} = - \left[m_{11}^2 \Phi_S^\dagger \Phi_S + m_{22}^2 \Phi_D^\dagger \Phi_D \right] / 2 + \left[\lambda_1 \left(\Phi_S^\dagger \Phi_S \right)^2 + \lambda_2 \left(\Phi_D^\dagger \Phi_D \right)^2 \right] / 2$, in a following way:

$$\mu_1 = m_{11}^2 / \sqrt{\lambda_1}, \quad \mu_2 = m_{22}^2 / \sqrt{\lambda_2}. \quad (3)$$

This phase diagram allowed us to present the possible types of evolution in easy way in form of rays. Each of the considered evolutions can be realized only if certain conditions for μ_1, μ_2 are satisfied. In the numerical analysis in [7] we have fixed the scalar masses, while the values of the scalar self-couplings λ_2 and λ_{345} were chosen to fulfil the constraints for each ray. In this work we focus on those couplings, mainly on the λ_2 parameter, which is a quartic coupling for the DM particles, usually neglected in analysis of $\Omega_{DM}h^2$. However, this parameter has an important impact on the evolution and the history of the Universe.

The content of this paper is as follows. In section 2 we present the main properties of IDM. In section 3 we discuss in details the DM relic density constrains in three regions of DM mass. In section 4 we introduce the $(\lambda_{345}, \lambda_2)$ plane, which is useful in the discussion of the parameter regions for different rays, at the fixed scalar masses. Here we use the benchmark points to illustrate three regions of DM mass and present the connection between the type of evolution and the values of $\Omega_{DM}h^2$. Section 5 contains a discussion on influence of different mass parameters on the $(\lambda_{345}, \lambda_2)$ regions along with the relic density values.

2 Model properties

2.1 IDM

Lagrangian We consider an electroweak symmetry breaking (EWSB) via the Brout-Englert-Higgs-Kibble (BEHK) mechanism described by the Lagrangian

$$\mathcal{L} = \mathcal{L}_{gf}^{SM} + \mathcal{L}_H + \mathcal{L}_Y(\psi_f, \Phi_S), \quad \mathcal{L}_H = T - V. \quad (4)$$

Here, \mathcal{L}_{gf}^{SM} describes the SM interaction of gauge bosons and fermions.

The Higgs scalar Lagrangian \mathcal{L}_H describes the interaction of two scalar doublets Φ_S and Φ_D with the standard kinetic term T and the scalar potential V . The potential V , which can describe IDM, is invariant under D -symmetry:

$$V = -\frac{1}{2} \left[m_{11}^2 \Phi_S^\dagger \Phi_S + m_{22}^2 \Phi_D^\dagger \Phi_D \right] + \frac{1}{2} \left[\lambda_1 \left(\Phi_S^\dagger \Phi_S \right)^2 + \lambda_2 \left(\Phi_D^\dagger \Phi_D \right)^2 \right] + \lambda_3 \left(\Phi_S^\dagger \Phi_S \right) \left(\Phi_D^\dagger \Phi_D \right) + \lambda_4 \left(\Phi_S^\dagger \Phi_D \right) \left(\Phi_D^\dagger \Phi_S \right) + \frac{1}{2} \lambda_5 \left[\left(\Phi_S^\dagger \Phi_D \right)^2 + \left(\Phi_D^\dagger \Phi_S \right)^2 \right]. \quad (5)$$

All parameters of (5) are real and one can fix $\lambda_5 < 0$ without a loss of generality.

In order to have a stable vacuum we impose *positivity constraints* in the following form:

$$\lambda_1 > 0, \quad \lambda_2 > 0, \quad R + 1 > 0, \quad (6)$$

$$\lambda_{345} = \lambda_3 + \lambda_4 + \lambda_5, \quad R = \lambda_{345} / \sqrt{\lambda_1 \lambda_2}. \quad (7)$$

They assure that the potential is bounded from below and the extremum with the lowest energy will be the vacuum (the global minimum of the potential).

D -symmetric potential has 7 independent real parameters: $m_{11}^2, m_{22}^2, \lambda_{1-5}$. After EWSB those parameters can be expressed by the non-zero v.e.v, four scalar masses and two self-couplings between scalars.

\mathcal{L}_Y describes the Yukawa interaction of fermions ψ_f with only one scalar doublet Φ_S . It has the same form as in the SM with the change $\Phi \rightarrow \Phi_S$ (Model I for Yukawa interaction). \mathcal{L}_Y respects D -symmetry in any order of the perturbation theory.

Inert vacuum We assume that the vacuum state of the potential (5) is given by the inert state (denoted by I_1). In this case only Φ_S acquires the non-zero vacuum expectation value, which as it follows from extremum condition is equal to:

$$v^2 = m_{11}^2/\lambda_1. \quad (8)$$

For I_1 to be the vacuum following conditions should be satisfied [6]:

$$\mu_1 > 0 \text{ for any } R, \quad \mu_1 > \mu_2 \text{ for } R > 1, \quad R\mu_1 > \mu_2 \text{ for } |R| < 1. \quad (9)$$

The inert vacuum state is invariant under the D -transformation just as the whole basic Lagrangian (4). There exist four dark scalar particles D_H, D_A, D^\pm , which are D -odd, and the Higgs particle h_S , which interacts with the fermions and gauge bosons just as the Higgs boson in the SM. h_S and the SM fields are D -even. In the inert vacuum the D -parity is conserved, and due to this fact the lightest D -odd particle is stable, being a good DM candidate.

The masses of the physical fields h_S, D_H, D_A and D^\pm can be used to express the parameters of V after EWSB. Those relations are given by:

$$\begin{aligned} M_{h_S}^2 &= \lambda_1 v^2 = m_{11}^2, & M_{D^\pm}^2 &= \frac{\lambda_3 v^2 - m_{22}^2}{2}, \\ M_{D_A}^2 &= M_{D^\pm}^2 + \frac{\lambda_4 - \lambda_5}{2} v^2, & M_{D_H}^2 &= M_{D^\pm}^2 + \frac{\lambda_4 + \lambda_5}{2} v^2. \end{aligned} \quad (10)$$

Other crucial parameters after EWSB are the couplings between the scalars. To complete the set of parameters we use two of them, λ_{345} and λ_2 . The λ_{345} is a coupling between SM-like Higgs h_S and DM candidate D_H : $D_H D_H h_S$ and $D_H D_H h_S h_S$. The λ_2 coupling is proportional to a *quartic* self-coupling among D -particles, e.g. $D_H D_H D_H D_H$. The self-coupling that governs the charged scalars' interactions: $D^+ D^- h_S$ and $D^+ D^- h_S h_S$ is proportional to λ_3 .

2.2 Collider constraints

Various theoretical and experimental constraints apply to the IDM (see e.g. [8, 9, 10, 11, 12, 13, 14, 15, 16, 17, 18]). Below we list important existing constraints on couplings and masses both for the Higgs particle and the dark scalars.

Constraints on self-couplings The positivity constraints are imposed directly on quartic parameters in the potential. If we want to assure the perturbativity of the theory, the self-couplings λ 's (i.e. $\lambda_2, \lambda_3, \lambda_{345}$) cannot be large. The bound (called perturbativity constraint) is set typically to

$$|\lambda| < 4\pi. \quad (11)$$

Electroweak precision tests EWPT constrain strongly physics beyond SM. In IDM they limit the allowed values of masses both for the Higgs particle h_S and the dark scalars. For IDM both light and heavy Higgs particle is allowed by EWPT [2]. Constraints for the dark scalars can be conveniently expressed by the limits for the mass splittings:

$$\delta_A = M_{D_A} - M_{D_H}, \quad \delta_{\pm} = M_{D^{\pm}} - M_{D_H}. \quad (12)$$

In [11] it was obtained that for a light Higgs boson, the allowed region corresponds to $\delta_{\pm} \sim \delta_A$ with mass splittings that could be large. For heavy SM Higgs large δ_{\pm} is needed, while δ_A could be small. In this work we limit ourselves to the light SM-like Higgs boson h_S .

LEP II limits As D^{\pm}, D_A, D_H do not couple to fermions, the LEP limits based on Yukawa interaction for the standard 2HDM don't apply. However, the signatures are similar to neutralinos and charginos interactions in MSSM. The absence of a signal within searches for supersymmetric neutralinos at LEP II was interpreted within the IDM in paper [17]. This analysis excludes the following region of masses: $M_{D_H} < 80$ GeV, $M_{D_A} < 100$ GeV and $\delta_A > 8$ GeV. For $\delta_A < 8$ GeV the LEP I limit $M_{D_H} + M_{D_A} > M_Z$ applies.

3 DM relic density constraints

In this analysis we assume that D_H is a dominant component of the observed DM, with its energy relic density in the Universe estimated to [19]:

$$\Omega_{DM} h^2 = 0.112 \pm 0.009. \quad (13)$$

Various studies show [11, 12, 13, 14, 15, 16] that for IDM in most regions of the parameter space $\Omega_{DM} h^2$ is too low to fulfil the astrophysical constraints. However, there are three allowed regions of M_{D_H} : (i) light DM particles with mass close to and below 10 GeV, (ii) medium DM mass of 40 – 80 GeV and (iii) heavy DM of mass larger than 500 GeV.

Those regions are further constrained by the value of λ_{345} , which governs the main decay channels (decay through Higgs exchange) for $M_{D_H} < M_W$. In general, for larger $|\lambda_{345}|$ the relic density decreases due to the enhanced $D_H D_H$ annihilation via h_S into pair of fermions (typically $\bar{b}b$).

On the contrary, the value of λ_2 does not influence the DM relic density directly. At the same time, this parameter is difficult to access at colliders. Therefore, this parameter is usually fixed to arbitrary small value in the DM analysis of IDM [11, 12, 13, 14, 15, 16]. However, as we argue in this paper, value of λ_2 limits the value of λ_{345} by the positivity constraints. Its value is also limited by the constraints arising from the possible existence of extrema and vacua of different properties than I_1 during the evolution of the Universe. Therefore, in this analysis we will consider the constraints for M_{D_H} as well as for both λ_{345} and λ_2 arising from the astrophysical data.

In this work we derive the corresponding relic-density constraints for IDM, using micrOMEGAs [20], with the IDM implemented by us. In analysis we respect all other existing limits and confirm findings of [11, 12, 13, 14, 15, 16]. The micrOMEGAs program neglects temperature dependence of physical parameters and a possibility of more than one phase transition. In paper [6] we concluded that if in the past there were sequences of phase transitions, then the Universe entered the inert phase with DM candidate at lower temperatures than in the typical one-stage EWSB. In principle, this should be considered while solving the Boltzmann equations for DM relic density, especially while the final phase transition into I_1 takes place at the low temperatures during the freeze-out. Also the latent heat of the 1st-order transition may give significant

corrections in some regions of the allowed parameter space [21]. In this sense, the energy relic density calculations in this paper should be considered only as a preliminary estimate.¹

Below we discuss the general trends in the change of $\Omega_{DM}h^2$ value in three regions of DM masses. In all examples we consider the light SM-like Higgs with its mass fixed to $M_h = 120$ GeV. We expect the $\Omega_{DM}h^2$ to be in the 3σ WMAP range, namely:

$$0.085 < \Omega_{DM}h^2 < 0.139. \quad (14)$$

Note, that the medium DM mass region is strongly constrained by the existing collider data.

3.1 Low DM mass region

In the low mass region M_{D_H} is of the order (4 – 8) GeV and masses of D_A and D^\pm are almost degenerate with $\delta_A \approx \delta_{H^\pm} \approx 100$ GeV [11].

Large mass splittings between the D_H and other scalar particles do not allow for the coannihilation. The main decay channel is $D_H D_H \rightarrow f \bar{f}$ ($c\bar{c}$ pair for $M_{D_H} = 4$ GeV and $b\bar{b}$ pair for higher M_{D_H}) via Higgs boson exchange. Small $|\lambda_{345}|$ generally gives high $\Omega_{DM}h^2$ well above the WMAP limit, as this decay channel is suppressed. The larger $|\lambda_{345}|$ is, the lower $\Omega_{DM}h^2$ gets. The WMAP allowed region of $|\lambda_{345}|$ is around (0.4, 1.2), but this strongly depends on the exact value of M_{D_H} (figure 1). Note, that the 1 GeV difference in mass is this region causes significant change in the $\Omega_{DM}h^2$ for a given λ_{345} .

One should remember that changing of λ_{345} is allowed only in the region allowed by the value of λ_2 (in the calculation of $\Omega_{DM}h^2$ we set $\lambda_2 = 5$ which corresponds to $1.5 > \lambda_{345} > -1.5$). In general, as we allow the higher values of λ_2 the range of λ_{345} , over which we can scan, extends and for a chosen M_{D_H} the higher $|\lambda_{345}|$ is the lower $\Omega_{DM}h^2$ we get.

For the low mass region relic density does not depend on the value of masses of the much heavier D_A and D^\pm . In our analysis we keep the mass splittings fixed to $\delta_A = 100$, $\delta_\pm = 105$ GeV and M_{D_H} changes in the allowed region (4 – 8) GeV. As M_{D_H} decreases, the value of relic density for the chosen λ_{345} grows, as shown in the figure 1.

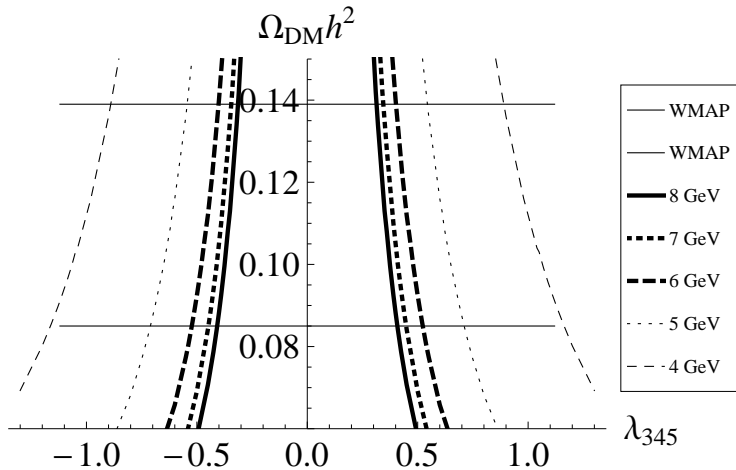


Figure 1: Relic density for $M_{D_H} = (4 - 8)$ GeV, $\lambda_2 = 5$, $\delta_A = 100$ GeV, $\delta_\pm = 105$ GeV. Horizontal lines denote WMAP 3σ allowed region.

¹More work is in progress.

3.2 Medium DM mass region

In the medium mass region the mass of D_H is in range $M_{D_H} = (30 - 80)$ GeV. Mass splittings δ_A, δ_{\pm} can be of the same order $\delta_A \approx \delta_{\pm} = (50 - 90)$ GeV, but also small values of δ_A are possible (of the order of 10 GeV) [11].

The medium mass region $\Omega_{DM}h^2$ is very sensitive to the value of M_{D_H} . Therefore in this case it is difficult to make a general statement similar to the low mass case (section 3.1). However, we see some regularities in this behaviour, related mostly with the effects of coannihilation, as discussed below. For our calculation we use $\lambda_2 = 0.3$, which in this mass range allows scanning over λ_{345} in range $\sim (-0.3, -0.35)$.

Small δ_A Let us first consider the small mass splitting between D_H and D_A (figure 2a):

$$\delta_A = 8 \text{ GeV} , \quad \delta_{H\pm} = 50 \text{ GeV} .$$

Small δ_A makes the coannihilation (D_H, D_A) important, decreasing the $\Omega_{DM}h^2$ below the WMAP limit in most of the λ_{345} parameter space. Usually only the region close to $\lambda_{345} = 0$ is inside the WMAP limit. For the larger masses of D_H , larger λ_{345} are allowed.

Note, that the smaller masses of D_H which may give a different results are heavily constrained by the LEP II data.

Large δ_A If mass splittings between D_H and other scalars are larger ($\delta \sim 50$ GeV) then the coannihilation is no longer important. For smaller masses and large mass splittings the behaviour is similar to the one in the low mass region (λ_{345} region around 0 is excluded and larger $|\lambda_{345}|$ are allowed, figure 2b). The allowed values of $|\lambda_{345}|$ are larger than in the case of small δ_A .

This region of masses is the most natural to consider as the constrains for the masses of scalars are not so tight as in other cases.

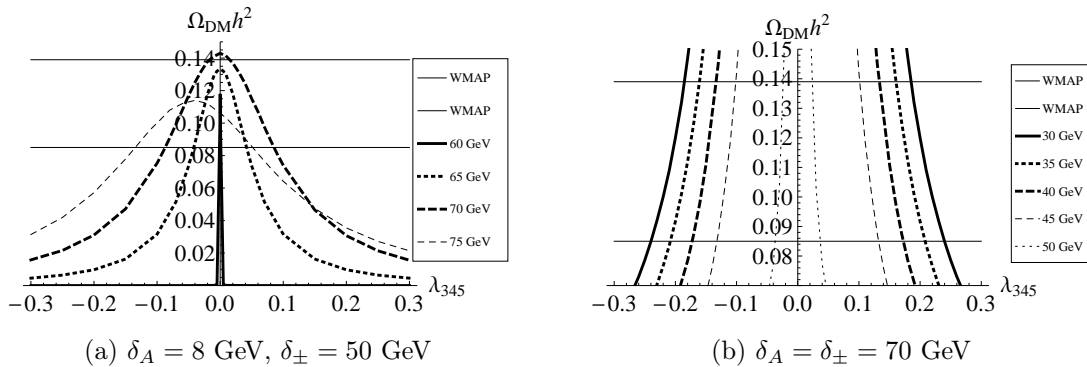


Figure 2: Relic density for medium mass region, results for $\lambda_2 = 0.3$.

3.3 High DM mass region

In the high mass region $M_{D_H} = (500 - 1000)$ GeV all dark scalars have almost degenerate masses and the mass splittings are small of the order of $\delta \approx \delta_A \approx \delta_{\pm} < 12$ GeV due to the perturbativity conditions [11].

In this high mass region, with such small mass splitting, the coannihilation between all dark scalars particles is very important. The results show very high sensitivity to the value of δ 's, as shown in figure 3. Here we fix $M_{D_H} = 800$ GeV, while δ varies from 1 to 10 GeV, respectively. In general, as δ grows, the value of relic density for given λ_{345} decreases. For $\delta = 10$ GeV, for every value of λ_{345} , we are below the WMAP limit.

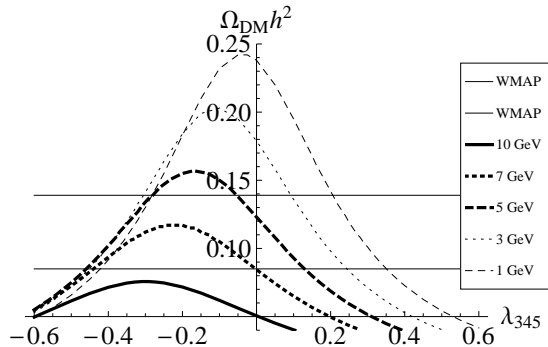


Figure 3: Relic density for high mass region: $(\lambda_{345}, \Omega_{DM}h^2)$ plot for fixed DM mass $M_{DH} = 800$ GeV and $\delta_{A,\pm} = (1, 3, 5, 7, 10)$ GeV, results for $\lambda_2 = 1.5$.

In figure 4 M_{DH} changes between 500 and 1000 GeV, while δ 's are fixed. We first consider $\delta = 1$ GeV (figure 4a), where lower values of M_{DH} correspond to the lower values of $\Omega_{DM}h^2$. If $\delta = 10$ GeV (figure 4b) then for most of the chosen values of M_{DH} we are below the WMAP limit. Mass around 1000 GeV gives the proper relic density for higher values of $|\lambda_{345}|$, note that $\lambda_{345} < 0$.

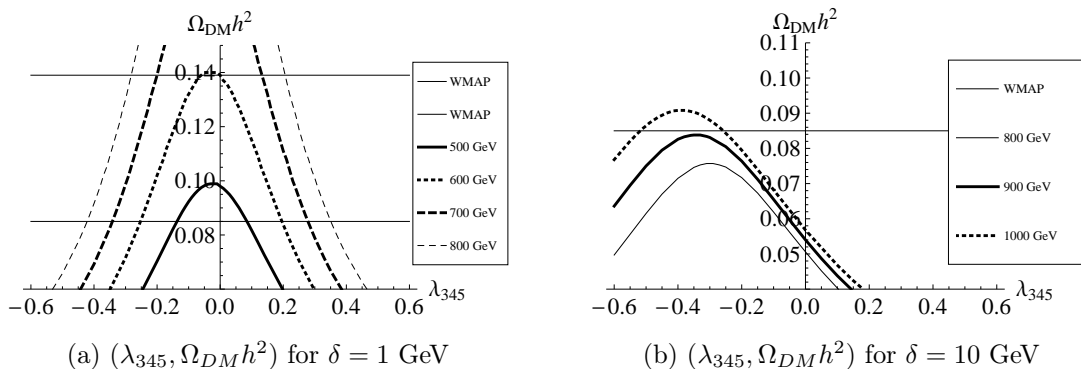


Figure 4: Relic density for high mass region for varied DM mass. Results for $\lambda_2 = 1.5$.

4 Thermal evolution

4.1 Thermal evolution of the Universe

Evolution of the potential Following the approach presented in [3, 4, 5, 6, 7] we consider the first nontrivial temperature corrections to the potential V . The coefficients λ 's of the quartic terms are unchanged, while the quadratic terms vary with temperature T with coefficients:

$$m_{11}^2(T) = m_{11}^2 - c_1 T^2, \quad m_{22}^2(T) = m_{22}^2 - c_2 T^2, \quad (15)$$

$$c_1 = \frac{3\lambda_1 + 2\lambda_3 + \lambda_4}{6} + \frac{3g^2 + g'^2}{8} + \frac{g_t^2 + g_b^2}{2}, \quad c_2 = \frac{3\lambda_2 + 2\lambda_3 + \lambda_4}{6} + \frac{3g^2 + g'^2}{8}.$$

The EW gauge couplings g and g' and Yukawa couplings for b and t quarks are:

$$g = 2M_W/v = 0.652, \quad g' = 0.351; \quad g_i = \sqrt{2}m_i/v \quad (g_t \approx 0.99, g_b \approx 0.02). \quad (16)$$

As shown in [6], depending on the value of λ 's each of the coefficients c_1 and c_2 can be either positive or negative. In this work we don't discuss the possibility of non-restoration of the EW symmetry in the past [22] and therefore we consider $c_2, c_1 > 0$ only [6].

| Extrema and vacua | | |
|---------------------------------|-----------------------------------------------------------|---------------------------------------------------------------------------------------------------------------------------------------------------------------------------|
| name of extremum | vev's | properties of vacuum |
| <i>EW symmetric: EWs</i> | $v_D = 0, \quad v_S = 0$ | Massless fermions and bosons and massive scalar doublets. |
| <i>inert: I₁</i> | $v_D = 0, \quad v_S^2 = v^2 = \frac{m_{11}^2}{\lambda_1}$ | Massive fermions and gauge bosons; scalar sector: SM-like Higgs h_S and dark scalars D_H, D_A, D^\pm with DM candidate D_H . |
| <i>inertlike: I₂</i> | $v_S = 0, \quad v_D^2 = v^2 = \frac{m_{22}^2}{\lambda_2}$ | Massless fermions and massive gauge bosons; scalar sector: Higgs particle h_D (no interaction with fermions), four scalars S_H, S_A, S^\pm , no DM candidate . |
| <i>mixed: M</i> | $v_S^2, v_D^2 > 0, \quad v^2 = v_S^2 + v_D^2$ | Massive fermions and bosons, 5 Higgs particles: CP-even h and H , CP-odd A and charged H^\pm , no DM candidate . |

Table 1: Extrema and properties of the vacua [6].

Extrema during the evolution Depending on the values of the parameters the D -symmetric potential (5) may have different types of the vacuum state. The general form of an neutral extremum is given by the following solution of the extremum conditions:

$$\langle \Phi_S \rangle = \frac{1}{\sqrt{2}} \begin{pmatrix} 0 \\ v_S \end{pmatrix}, \quad \langle \Phi_D \rangle = \frac{1}{\sqrt{2}} \begin{pmatrix} 0 \\ v_D \end{pmatrix}, \quad (v^2 = v_S^2 + v_D^2). \quad (17)$$

The properties of these extrema, provided they are realized as vacua, are listed in the table 1. As we discussed in [6], each of this vacua can be realized in the separate regions in (μ_1, μ_2) plane.

Types of evolution As the quadratic terms in V vary with T , the vacuum state changes. As time grows (and temperature decreases) the vacuum state of the Universe changes along one of rays in the phase diagrams shown in figure 5, where the allowed regions for all vacua EWs , I_1 , I_2 and M are shown as well.

The types of evolution (rays), along with conditions on R and μ_1, μ_2 that need to be satisfied in order to have a chosen type of evolution, are summarised in the table 2 in the appendix. Note, that in existing in literature DM analysis only the rays that correspond to a single phase transition $EWs \rightarrow I_1$ have been considered.

4.2 Rays in the $(\lambda_{345}, \lambda_2)$ plane

To get a deeper insight into evolution of the Universe we consider now parametrization of rays by the physical parameters like masses and self-couplings. We will use the $(\lambda_{345}, \lambda_2)$ plane, to represent regions where a certain ray is realized, treating masses of scalars $M_{h_s}, M_{D_H}, M_{D_A}, M_{D^\pm}$ as the input parameters. Conditions from table 2 have been translated into conditions for $(\lambda_{345}, \lambda_2)$ parameters and are presented in table 3 in the appendix. Note, that only for the case of a single phase transition we need to impose the constraints for λ_{345} parameter. In case

of sequences with two or three phase transitions, constraints on the quartic coupling λ_2 are sufficient.

The $(\lambda_{345}, \lambda_2)$ phase space can be divided into separate sectors. Let us introduce $\tilde{\lambda}_{345}$ parameter, which separates these sectors:

$$\tilde{\lambda}_{345} = \frac{2M_{D_H}^2}{v^2}. \quad (18)$$

For $\lambda_{345} < \tilde{\lambda}_{345}$, which corresponds to $\mu_2 < 0$, the only EWv extremum, and thus the vacuum, that ever existed is the inert phase I_1 . The only possible sequence is $EWs \rightarrow I_1$. For $\lambda_{345} > \tilde{\lambda}_{345}$ ($\mu_2 > 0$) other EWv extrema (M, I_2) could be realized in the past. Their realization as vacua depends on the value of λ_2 .

Distinct regions of λ_2 are separated by $\tilde{\lambda}_2$, which depends on λ_{345} and other parameters as follows:

$$\tilde{\lambda}_2 = \frac{-(3g^2 + g'^2)}{4} - \frac{(M_{D_A}^2 - 3M_{D_H}^2 + 2M_{D^\pm}^2)}{3v^2} + \frac{\lambda_{345}}{3} + \frac{(2M_{D_H}^2 - v^2\lambda_{345})}{12} \times \frac{(-4M_{D_A}^2 + 12M_{D_H}^2 - 8M_{D^\pm}^2 - (9g^2 + 3g'^2 + 12g_b^2 + 12g_t^2 + 8\lambda_{345})v^2)}{v^2M_{h_s}^2}. \quad (19)$$

Note, that for $\lambda_2 > \tilde{\lambda}_2$ only one phase transition may be realized, while for $\lambda_2 < \tilde{\lambda}_2$ sequences with two or three phase transitions are possible.

Below we perform a general analysis of possible rays on the $(\lambda_{345}, \lambda_2)$ plane for various masses, assuming that today I_1 vacuum is realized.

4.3 Benchmark points

For further discussions we will use the reference points $B1 - B4$ chosen in three regions of M_{D_H} as follows. For all points $M_{h_s} = 120$ GeV.

- Low DM mass region: for the reference point $B1$ we have:

$$B1 : \quad M_{D_H} = 8 \text{ GeV}, \delta_A = 100 \text{ GeV}, \delta_{\pm} = 105 \text{ GeV}. \quad (20)$$

- Medium DM mass region: as discussed, large or small δ_A are possible. Those are the benchmark points $B2$ and $B3$, respectively.

$$B2 : \quad M_{D_H} = 45 \text{ GeV}, \delta_A = 70 \text{ GeV}, \delta_{H^\pm} = 70 \text{ GeV}, \quad (21)$$

$$B3 : \quad M_{D_H} = 70 \text{ GeV}, \delta_A = 8 \text{ GeV}, \delta_{H^\pm} = 50 \text{ GeV}. \quad (22)$$

- The high DM mass region set $B4$ is defined as:

$$B4 : \quad M_{D_H} = 800 \text{ GeV}, \delta_A = 1 \text{ GeV}, \delta_{H^\pm} = 1 \text{ GeV}. \quad (23)$$

Figures (6a-d) show the regions, where concrete rays can be realized in $(\lambda_{345}, \lambda_2)$ plane for mass points $B1 - B4$.² In general, the higher D_H mass is, the higher values of λ_{345} are needed for the realization of the sequences with more than one phase transition. More discussion is given below (sec. 4.4-4.6), where also the relic density as the function of λ_{345} is discussed.

²Note, that the scales in those figures are different.

4.4 Low DM mass region

Rays in $(\lambda_{345}, \lambda_2)$ plane Figure 6a shows the $(\lambda_{345}, \lambda_2)$ plane for the low mass point $B1$. In this case possible types of evolution are very limited. There is an allowed region for the single phase transition (realized by ray Ic for $R < 0$ and ray IIb for $1 > R > 0$) and sequence of three phase transitions with transition through M (ray VI). Important feature of this low DM mass region is the fact that 1st-order phase transition $EWs \rightarrow I_2 \rightarrow I_1$ is not possible (rays IV and V), as the allowed phase space for those rays shrinks to the degenerate line $\lambda_2 \approx \lambda_{345}^2 v^2 / M_{h_s}^2$. In short, fulfilling $R > 1$ condition is not possible for the low DM mass region.

Relic density The obtained energy relic density as a function of λ_{345} is presented in figure 7a for a low mass benchmark point B1. There are two regions in agreement with the WMAP limit: $\lambda_{345} \in (-0.405, -0.315)$ and $\lambda_{345} \in (0.315, 0.405)$, presented as the dark regions in $(\lambda_2, \lambda_{345})$ plot (figure 7b). For the negative values of λ_{345} ray Ic, for positive – ray VI or ray IIb, depending on the value of λ_2 , can be realized. Note, that the value of λ_2 should be quite large to have any kind of solution that fits into the WMAP region. Because of the positivity constraints for $\lambda_{345} \in (-0.405, -0.315)$ we need $\lambda_2 > 0.45$ if we want to have ray Ic.³ For $\lambda_{345} > 0$ and $1.9 > \lambda_2 > 0.45$ only ray VI is realized; if we want to have ray IIb we need $\lambda_2 > 1.9$.

Calculation of $\Omega_{DM} h^2$ was done for $\lambda_2 = 5$, which does not influence its value. However, as we discussed above, the value of λ_2 is limited by the other constrains for certain rays. It is limited by the positivity constraints $\lambda_{345} + \sqrt{\lambda_1 \lambda_2} > 0$ for $\lambda_{345} < 0$, while for $\lambda_{345} > 0$ positivity constraints don't give the further constraints on λ_2 , but its value is limited by the conditions of realization of particular rays (table 3).

4.5 Medium mass region

Rays in $(\lambda_{345}, \lambda_2)$ plane Figure 6b shows the allowed rays for the reference point $B2$ in the medium mass region for $M_{D_H} = 45$ GeV. In this case all types of evolution are possible. Note, that rays that correspond to the sequence of two or more phase transitions (rays IV, V and VI) appear for larger values of λ_{345} . For the point $B3$, with $M_{D_H} = 70$ GeV, the types of rays are similar to the $B2$ case, as shown in figure 6c. Some small differences are visible, for example ray VI requires larger value of λ_2 . Those differences are mainly due to the value of M_{D_H} , mass splittings δ_A, δ_{\pm} are less important (see section 5).

Relic density Point $B2$ is similar to the low mass region as here the coannihilation is not relevant. However, due to the larger D_H mass the annihilation through Higgs exchange is more efficient and the obtained λ_{345} values are smaller. Again there are two allowed regions that give the proper relic density (figure 8). Note, that this time for the positive λ_{345} rays IIb, IIa and III (the later with the coexisting local minimum I_2) are allowed by the relic density data.

In case of the point $B3$ due to the small value of δ_A the coannihilation (D_H, D_A) is important for the relic density. Its effects are clearly visible for the very small values of λ_{345} , where annihilation through Higgs is strongly suppressed (figure 9a). We get the proper relic density for $\lambda_{345} \in (-0.1, 0.1)$ with the small region around 0 excluded. This corresponds to rays Ia-c, depending on the value of λ_2 (figure 9b). Here, sequences with more than one phase transition give $\Omega_{DM} h^2$ below the WMAP limit.

³For positive allowed λ_{345} and $\lambda_2 < 0.45$ the Universe is in the state of intertlike vacuum.

4.6 High mass region

Rays in $(\lambda_{345}, \lambda_2)$ plane For small values of λ_{345} only rays Ic, Ib and Ia are possible (figure 6d). The types of evolution other than a single phase transition could happen only for the very large values of $\lambda_{345} > 2M_{D_H}^2/v^2$, which for $M_{D_H} = O(800)$ GeV gives $\lambda_{345} = O(20)$.

Relic density In high DM mass region, due to the very small mass splittings coannihilation processes are the most important ones. For chosen set of masses the allowed ranges of λ_{345} are $(-0.42, -0.28)$, $(0.21, 0.35)$, as shown in figure 10a. It is clear that for this set the allowed rays are Ia, Ib, Ic (single phase transitions). The other rays could be realized for $\lambda_3 > 22$, but first of all, it would violate the perturbativity constraints. On the other hand, the value of $\Omega_{DM}h^2$ is very low (of the order of 10^{-3}) for such large λ_3 (and λ_{245}).

5 Sensivity of the types of evolution to the dark scalar masses

The realization of different types of evolution depends strongly on values of all parameters in the potential, as presented in numerical examples in [7]. However, in general the value of M_{D_H} affects the type of evolution stronger than the values of M_{D_A} and $M_{D_{\pm}}$.

Let us consider first the values of masses for dark scalars allowed by the relic density constraints for the low and medium mass of $M_{D_H} \approx (8 - 80)$ GeV:

$$M_{D_A} = 110 \text{ GeV}, \quad M_{D_{\pm}} = 110 \text{ GeV}. \quad (24)$$

Figures (11a-d) show the regions of parameters on $(\lambda_{345}, \lambda_2)$ for the different values of M_{D_H} (from 8 GeV to 60 GeV). For the low mass region single phase transition (rays Ic, IIb) and transition through M vacuum (ray VI) are possible, other types of evolution appear for the higher values of M_{D_H} . As the mass grows, the region of ray IIa expands and thus ray VI becomes possible for the larger values of λ_2 .

If we fix the value of M_{D_H} and let the other masses vary (figures 13a-d) the picture is not significantly affected. This is presented in the example of the large mass splittings δ_A, δ_{\pm} , however using small δ_A doesn't make much difference (compare with figure 14a noticing the difference in scales).

Low DM mass region Since M_{D_H} is small compared to the other masses, $R > 1$ is in fact not possible and the possibilities presented in table 3 are reduced to only three rays (Ic, IIa, VI). In the considered range of M_{D_H} the main mass parameter that influences the boundaries of rays is mass of the Higgs, M_{h_S} . Changing M_{D_H} in the allowed range with fixed δ_A, δ_{\pm} for this region does not change the picture 6a. Boundary line between rays IIb and VI depends mostly on M_{h_S} and fixed gauge and Yukawa couplings. Small corrections ($\Delta\lambda_{345} = 0.01$) coming from the change of δ_A and δ_{\pm} arise for the small ($\lambda_2 \in (0.01, 0.1)$) and large ($\lambda_2 > 5$) values of λ_2 .

In section 3 we presented the $\Omega_{DM}h^2$ calculations for this region. Here we see that the values of M_{D_H} and λ_2 are the most important parameters. In a way, λ_2 is more important than λ_{345} , because even if we are in the allowed region of λ_{345} , the small value of λ_2 may lead us to a region excluded by the positivity constraints. As M_{D_H} grows, we enter the WMAP region for the lower absolute values of λ_{345} which corresponds to lower values of λ_2 (figure 12).

Medium DM mass region For large mass splittings $\delta_A \sim \delta_{\pm}$ all rays (and all types of evolution) are possible in the range $M_{D_H} = (30 - 60)$ GeV (figures 6b,11b-d). As mass grows, ray VI requires higher values of λ_2 and the region of this ray shrinks in benefit of rays IIa, IV and V. For the medium mass region the change of M_{D_H} effects the evolution for low values of λ_2 more than the change of M_{D_A} and $M_{D_{\pm}}$ for fixed value of M_{D_H} (figures 13a-d).

For small δ_A the picture is similar to the previous one, however as the M_{D_H} grows the allowed region of ray VI becomes limited in benefit of rays IIa and IV. For $M_{D_H} = 80$ GeV ray VI is still possible but it requires higher values of $\lambda_2 \approx 0.7$ (figures 14a-c).

The types of rays that may be realized with the λ_{345} inside the WMAP limit depend heavily on the specific value of M_{D_H} .

For small δ_A region around $\lambda_{345} = 0$ gives proper $\Omega_{DM}h^2$. Here only sequences with a single phase transition can be realized. As M_{D_H} grows, larger λ_{345} are allowed by WMAP. However, also the region where the more complex sequences can be realized shifts towards even larger λ_{345} (figure 14). In general, this case may provide us only the $EWs \rightarrow I_1$ sequences in agreement with WMAP (figure 15).

For large δ_A also sequences III-VI can be realized with the proper relic density (figure 16). This is the case for masses $M_{D_H} \approx 40$ GeV, where rays with the 1st-order phase transition are possible. For this value of mass the WMAP allowed range is in $\lambda_{345} \in (0.13, 0.17)$. One should keep in mind that this region can be constrained soon by the DM direct detection data. For larger masses the region of those complex sequences is shifted towards the larger values of λ_{345} . In general they give $\Omega_{DM}h^2$ below the WMAP limit due to the $D_H D_H \rightarrow h_S \rightarrow \bar{b}b$ channel. In this case we are left only with the $EWs \rightarrow I_1$ sequences realized for smaller λ_{345} inside WMAP limit.

High DM mass region In this region the lower value of M_{D_H} makes the realization of other than a single-phase transition types evolution possible for lower values of λ_{345} . Still, for $M_{D_H} = 500$ GeV this value is high of the order $O(10)$. If we limit ourselves to $\lambda_i \approx O(1)$ then only single phase transition is possible in the high mass region and the $(\lambda_{345}, \lambda_2)$ plot is virtually identical to figure 6d. As discussed before, proper $\Omega_{DM}h^2$ is for $\lambda_{345} < O(1)$ and thus the complex sequences are not in agreement with WMAP.

6 Conclusions and outlook

In this work we analysed the possible types of evolution of the Universe (rays) in the IDM, including constraints from the DM relic density data (WMAP). Three regions of the allowed dark matter masses: low, medium and high mass were considered. Evolution was parametrized by masses of scalars (including dark matter particle) and two parameters (self-couplings) λ_{345} and λ_2 . With fixed scalar masses we can find the values of $(\lambda_{345}, \lambda_2)$ that satisfy the conditions of a chosen ray (table 3 in the appendix). We have shown that those three regions of DM mass exhibit the different behaviour: both in the possible types of evolution and the energy relic density values.

For the low DM mass region only three kinds of rays can be realized: ray Ic, IIb and VI. This is due to the very low D_H mass and the exact values of the much heavier other scalars do not affect the picture. The energy relic density also doesn't depend on M_{D_A} or $M_{D_{\pm}}$, but it is strongly influenced by the exact value of M_{D_H} . In general, rather larger $|\lambda_{345}| \sim (0.4 - 1)$ are needed to fulfill the WMAP constraints. Due to this fact, in our approximation of the $\Omega_{DM}h^2$ calculation, sequence $EWs \rightarrow I_2 \rightarrow M \rightarrow I_1$ gives the proper $\Omega_{DM}h^2$.

For the medium DM mass region all types of evolutions are possible. Again the main parameter that affects the regions in $(\lambda_{345}, \lambda_2)$ plane is the mass of DM particle, however for lower λ_2 also the effect of changing of $M_{D_A}, M_{D_{\pm}}$ are visible. In this region $\Omega_{DM}h^2$ depends heavily on the value of M_{D_H} , but also on δ_A . There are two separate regions. For small δ_A coannihilation is possible and in general small $|\lambda_{345}|$ give the proper DM relic density. Large δ_A case is similar to the low DM mass case as the coannihilation is not important and the allowed $|\lambda_{345}|$ tends to shift towards the larger values.

In the high DM mass region all dark scalars have almost degenerate and very large masses. This has two main consequences. First, the $(\lambda_{345}, \lambda_2)$ plane for $\lambda < O(1)$ is reduced only to the regions corresponding to the simple sequences with a single phase transition. Second, the energy relic density is strongly lowered for most values of $|\lambda_{345}|$, because of the coannihilation.

We would like to comment, that the high mass region requires very careful fixing of the parameters, as it is very sensitive to changing the values of δ 's. This certainly doesn't seem to be natural (*fine-tuning*). From this point of view the most interesting is the medium mass region with the large mass splittings, as here the adjustment of the parameters isn't so strict.

It is worth to stress the importance of the often neglected λ_2 self-coupling. We argue, that the astrophysical data should be used to limit the values of this self-coupling. Firstly, the $\Omega_{DM}h^2$ calculation for a fixed M_{D_H} gives the allowed values of the λ_{345} parameter. This calculation doesn't depend on the exact value of λ_2 . Secondly, those obtained values of λ_{345} should be used to constrain the λ_2 parameter through the positivity constraints or the conditions for the realization of the different rays. Therefore, fixing λ_2 to an arbitrary value during the calculations may result in the exclusion of the WMAP allowed region. This is especially visible in the low and high DM mass region, where for the $\lambda_{345} < 0$ the positivity constraints require $\lambda_2 > (0.2 - 0.6)$.

As we mentioned in section 3, the calculations of $\Omega_{DM}h^2$ in this work should be treated only as an estimate. We do not take into account the corrections to those calculations arising from the thermal evolution of the Universe, such as the influence of complex sequences of phase transitions or the effect of the 1-st order phase transitions. Also, in certain ranges of $(\lambda_{345}, \lambda_2)$ for low and medium DM mass region the final phase transition into inert vacuum may take place at the lower temperatures, which may affect the freeze-out. Those effects are now under investigation.

Acknowledgments I would like to thank I. Gizburg, K. Kanishev and M. Krawczyk for cooperation and discussions. I would like to thank M. Krawczyk for reading the manuscript. Work was partly supported by Polish Ministry of Science and Higher Education Grant N N202 230337.

A Conditions for rays

Below we present the tables that contain the conditions for the realization of different types of evolution presented in two planes: (μ_1, μ_2) in table 2 and $(\lambda_{345}, \lambda_2)$ in table 3. Here we use the redefined evolution coefficient:

$$\tilde{c} = \tilde{c}_2/\tilde{c}_1 = (c_2\sqrt{\lambda_1})/(c_1\sqrt{\lambda_2}). \quad (25)$$

To make the table more transparent we use the previously introduced boundary values $\tilde{\lambda}_2, \tilde{\lambda}_{345}$:

$$\begin{aligned} \tilde{\lambda}_2 = & \frac{-(3g^2 + g'^2)}{4} - \frac{(M_{D_A}^2 - 3M_{D_H}^2 + 2M_{D_{\pm}}^2)}{3v^2} + \frac{\lambda_{345}}{3} + \frac{(2M_{D_H}^2 - v^2\lambda_{345})}{12} \times \\ & \times \frac{(-4M_{D_A}^2 + 12M_{D_H}^2 - 8M_{D_{\pm}}^2 - (9g^2 + 3g'^2 + 12g_b^2 + 12g_t^2 + 8\lambda_{345})v^2)}{v^2M_{h_s}^2}. \end{aligned} \quad (26)$$

| Ray no. | R | Conditions |
|-----------------------------------------------------|--------------|-------------------------------------------------------------|
| $EWs \rightarrow I_1$ | | |
| Ia | $R > 1$ | $\mu_2 < 0$ |
| IIa | $R > 1$ | $0 < \mu_2 < \text{Min}(\mu_1 \tilde{c}, \mu_1 R^{-1})$ |
| III | $R > 1$ | $\mu_1 R^{-1} < \mu_2 < \text{Min}(\mu_1 \tilde{c}, \mu_1)$ |
| Ib | $1 > R > 0$ | $\mu_2 < 0$ |
| IIb | $1 > R > 0$ | $0 < \mu_2 < \text{Min}(\mu_1 \tilde{c}, \mu_1 R)$ |
| Ic | $0 > R > -1$ | $\mu_2 < \mu_1 R < 0$ |
| $EWs \rightarrow I_2 \rightarrow I_1$ | | |
| IV | $R > 1$ | $\mu_1 \tilde{c} < \mu_2 < \mu_1 R^{-1}$ |
| V | $R > 1$ | $\text{Max}(\mu_1 \tilde{c}, \mu_1 R^{-1}) < \mu_2 < \mu_1$ |
| $EWs \rightarrow I_2 \rightarrow M \rightarrow I_1$ | | |
| VI | $1 > R > 0$ | $\mu_1 \tilde{c} < \mu_2 < \mu_1 R$ |

Table 2: Possible rays ; (μ_1, μ_2) conditions.

$$\tilde{\lambda}_{345} = \frac{2M_{DH}^2}{v^2} \quad (27)$$

and the abbreviation:

$$\alpha = \frac{(v^2 \lambda_{345} - 2M_{DH}^2)}{M_{hs}^2} \quad (28)$$

References

- [1] N. G. Deshpande and E. Ma, "Pattern Of Symmetry Breaking With Two Higgs Doublets," Phys. Rev. D **18** (1978) 2574.
- [2] R. Barbieri, L. J. Hall and V. S. Rychkov, "Improved naturalness with a heavy Higgs: An alternative road to LHC physics," Phys. Rev. D **74** (2006) 015007 [arXiv:hep-ph/0603188].
- [3] I. F. Ginzburg and K. A. Kanishev, "Different vacua in 2HDM," Phys. Rev. D **76** (2007) 095013 [arXiv:0704.3664 [hep-ph]].
- [4] I. F. Ginzburg, I. P. Ivanov and K. A. Kanishev, "The evolution of vacuum states and phase transitions in 2HDM during cooling of Universe," Phys. Rev. D **81** (2010) 085031 [arXiv:0911.2383 [hep-ph]].
- [5] I. P. Ivanov, "Thermal evolution of the ground state of the most general 2HDM," Acta Phys. Polon. B **40** (2009) 2789 [arXiv:0812.4984 [hep-ph]].

| Ray no. | λ_{345} region | λ_2 region |
|-----------------------------------------------------|---------------------------------------------|-------------------------------------------------------------------------------------------------------------------------|
| $EWs \rightarrow I_1$ | | |
| Ia | $0 < \lambda_{345} < \tilde{\lambda}_{345}$ | $\lambda_2 > \frac{\lambda_{345}^2 v^2}{M_{h_s}^2}$ |
| IIa | $\lambda_{345} > \tilde{\lambda}_{345}$ | $\text{Max} \left(\tilde{\lambda}_2, \alpha \lambda_{345} \right) < \lambda_2 < \frac{\lambda_{345}^2 v^2}{M_{h_s}^2}$ |
| III | | $\text{Max} \left(\tilde{\lambda}_2, \frac{\alpha^2 M_{h_s}^2}{v^2} \right) < \lambda_2 < \alpha \lambda_{345}$ |
| Ib | $0 < \lambda_{345} < \tilde{\lambda}_{345}$ | $\lambda_2 > \frac{\lambda_{345}^2 v^2}{M_{h_s}^2}$ |
| IIb | $\lambda_{345} > \tilde{\lambda}_{345}$ | $\text{Max} \left(\tilde{\lambda}_2, \frac{\lambda_{345}^2 v^2}{M_{h_s}^2} \right) < \lambda_2$ |
| Ic | $\lambda_{345} < 0$ | $\lambda_2 > \frac{\lambda_{345}^2 v^2}{M_{h_s}^2}$ |
| $EWs \rightarrow I_2 \rightarrow I_1$ | | |
| IV | | $\alpha \lambda_{345} < \lambda_2 < \text{Min} \left(\tilde{\lambda}_2, \frac{\lambda_{345}^2 v^2}{M_{h_s}^2} \right)$ |
| V | | $\frac{\alpha^2 M_{h_s}^2}{v^2} < \lambda_2 < \text{Min} \left(\tilde{\lambda}_2, \alpha \lambda_{345} \right)$ |
| $EWs \rightarrow I_2 \rightarrow M \rightarrow I_1$ | | |
| VI | | $\frac{\lambda_{345}^2 v^2}{M_{h_s}^2} < \lambda_2 < \tilde{\lambda}_2$ |

Table 3: Possible rays; $(\lambda_{345}, \lambda_2)$ conditions.

- [6] I. F. Ginzburg, K. A. Kanishev, M. Krawczyk and D. Sokolowska, “Evolution of Universe to the present inert phase,” *Phys. Rev. D* **82**, 123533 (2010) [arXiv:1009.4593 [hep-ph]].
- [7] D. Sokolowska, “Temperature evolution of physical parameters in the Inert Doublet Model,” arXiv:1104.3326 [hep-ph]
- [8] Q. H. Cao, E. Ma and G. Rajasekaran, “Observing the Dark Scalar Doublet and its Impact on the Standard-Model Higgs Boson at Colliders,” *Phys. Rev. D* **76** (2007) 095011 [arXiv:0708.2939 [hep-ph]].
- [9] P. Agrawal, E. M. Dolle and C. A. Krenke, “Signals of Inert Doublet Dark Matter in Neutrino Telescopes,” *Phys. Rev. D* **79**, 015015 (2009) [arXiv:0811.1798 [hep-ph]].
- [10] M. Gustafsson, E. Lundstrom, L. Bergstrom and J. Edsjo, “Significant gamma lines from inert Higgs dark matter,” *Phys. Rev. Lett.* **99** (2007) 041301 [arXiv:astro-ph/0703512].
- [11] E. M. Dolle and S. Su, “The Inert Dark Matter,” *Phys. Rev. D* **80** (2009) 055012 [arXiv:0906.1609 [hep-ph]].
- [12] E. Dolle, X. Miao, S. Su and B. Thomas, “Dilepton Signals in the Inert Doublet Model,” *Phys. Rev. D* **81**, 035003 (2010) [arXiv:0909.3094 [hep-ph]].
- [13] L. Lopez Honorez, E. Nezri, J. F. Oliver and M. H. G. Tytgat, “The inert doublet model: An archetype for dark matter,” *JCAP* **0702** (2007) 028 [arXiv:hep-ph/0612275].
- [14] C. Arina, F. S. Ling and M. H. G. Tytgat, “IDM and iDM or The Inert Doublet Model and Inelastic Dark Matter,” *JCAP* **0910**, 018 (2009) [arXiv:0907.0430 [hep-ph]].
- [15] M. H. G. Tytgat, “The Inert Doublet Model : a new archetype of WIMP dark matter?,” *J. Phys. Conf. Ser.* **120** (2008) 042026 [arXiv:0712.4206 [hep-ph]].
- [16] L. L. Honorez and C. E. Yaguna, “The inert doublet model of dark matter revisited,” arXiv:1003.3125 [hep-ph].
- [17] E. Lundstrom, M. Gustafsson and J. Edsjo, “The Inert Doublet Model and LEP II Limits,” *Phys. Rev. D* **79** (2009) 035013 [arXiv:0810.3924 [hep-ph]].
- [18] M. Krawczyk and D. Sokołowska, “Constraining the Dark 2HDM,” arXiv:0911.2457 [hep-ph].
- [19] Particle Data Group. *Journ. of Phys.* **G 37** #7A (2010) 075021.
- [20] G. Belanger, F. Boudjema, P. Brun, A. Pukhov, S. Rosier-Lees, P. Salati and A. Semenov, “Indirect search for dark matter with micrOMEGAs2.4,” *Comput. Phys. Commun.* **182**, 842 (2011) [arXiv:1004.1092 [hep-ph]].
- [21] I. Ginzburg (private communication); I. Ginzburg, K. Kanishev, M. Krawczyk, D. Sokołowska (work in progress).
- [22] M. B. Gavela, O. Pene, N. Rius and S. Vargas-Castrillon, “The fading of symmetry non-restoration at finite temperature,” *Phys. Rev. D* **59** (1999) 025008 [arXiv:hep-ph/9801244].

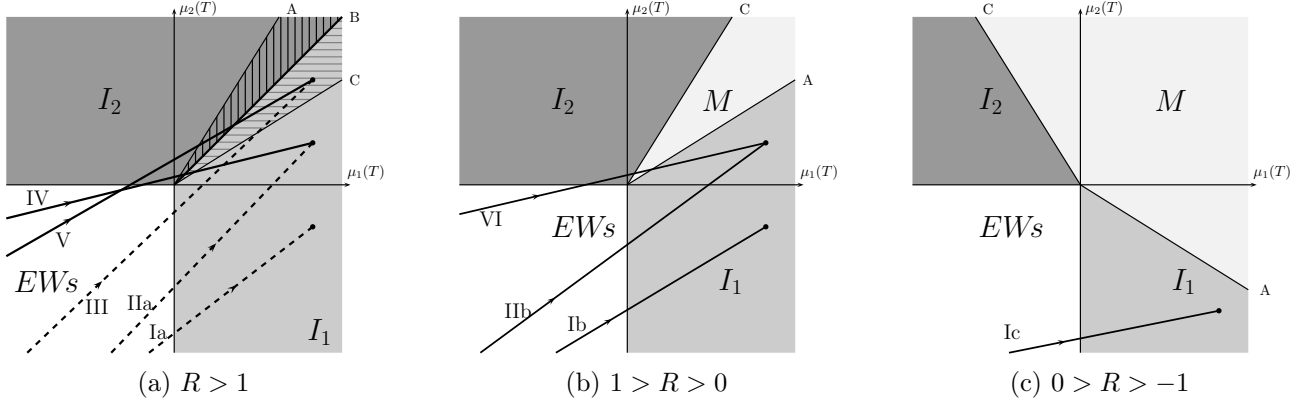


Figure 5: Possible rays on (μ_1, μ_2) plane. Vacua: EW symmetric (white region), inert (yellow, lightest shade), inertlike (blue, dark shade) and mixed (green, medium shade). Vertical hatch between lines A and B in figure 5a denotes the area when I_1 is a local minimum, while I_2 is the global one; horizontal hatch between B and C – I_2 is a local minimum, while I_1 is the vacuum.

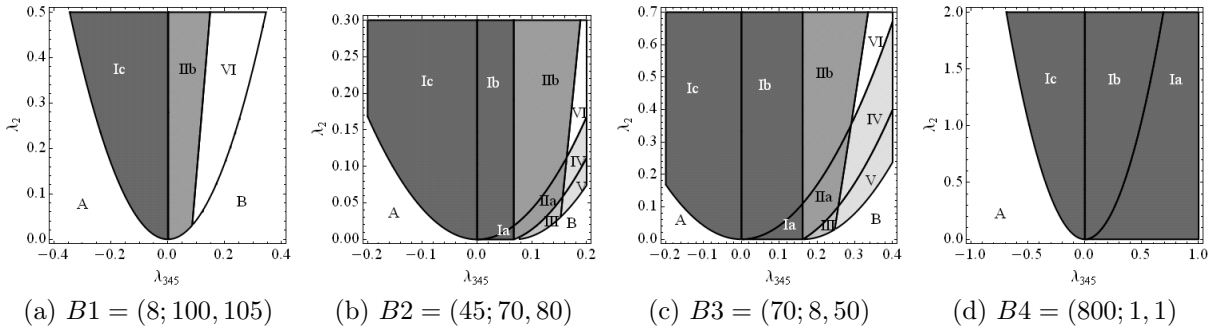


Figure 6: Regions of rays for reference points $B_i = (M_{DH}; \delta_A, \delta_{\pm})$ GeV for $M_{h_S} = 120$ GeV. Different colours correspond to the different rays. $EWs \rightarrow I_1$: Ia, Ib, Ib, IIa, IIb, III; $EWs \rightarrow I_2 \rightarrow I_1$: IV and V; $EWs \rightarrow I_2 \rightarrow M \rightarrow I_1$: VI. Region A excluded by positivity constraints, region B excluded by I_2 vacuum.

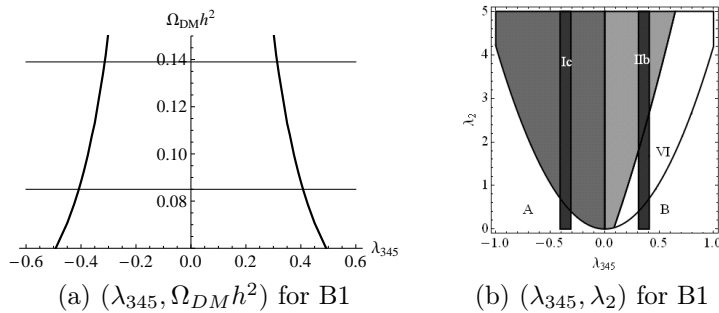


Figure 7: Relic density for $B1$ with $M_{DH} = 8$ GeV, $\delta_A = 100$ GeV, $\delta_{\pm} = 105$ GeV.

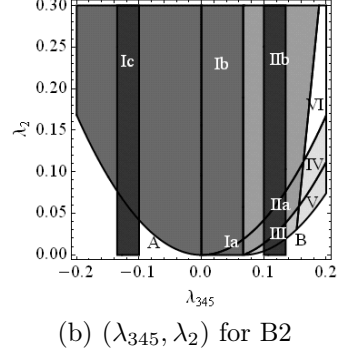
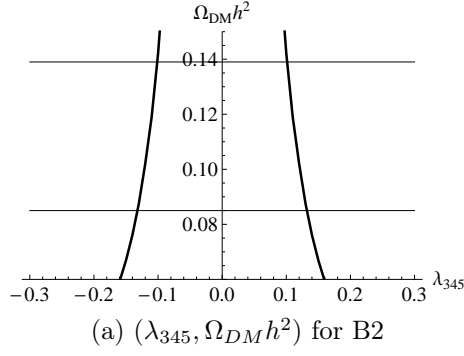


Figure 8: Relic density for $B2$ with $M_{D_H} = 45$ GeV, $\delta_A = \delta_{\pm} = 70$ GeV.

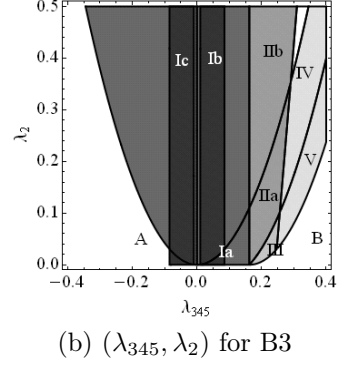
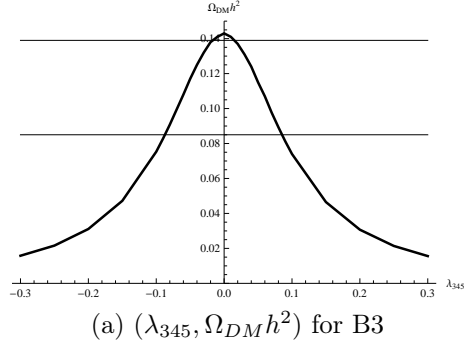


Figure 9: Relic density for $B3$ with $M_{D_H} = 70$ GeV, $\delta_A = 8$ GeV, $\delta_{\pm} = 50$ GeV.

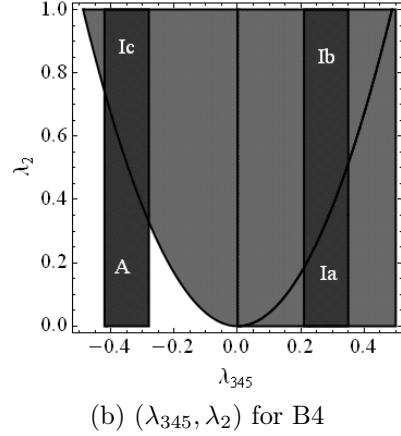
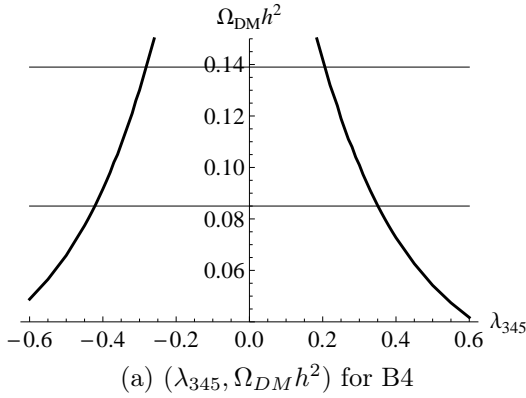


Figure 10: Relic density for $B4$ with $M_{D_H} = 800$ GeV, $\delta_{A,\pm} = 1$ GeV.

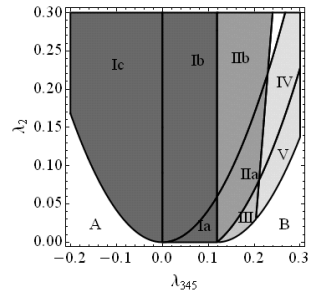
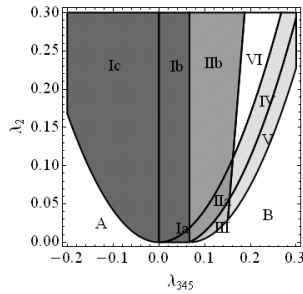
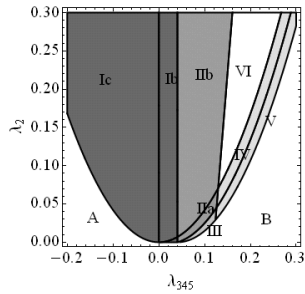
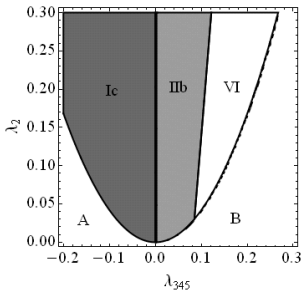


Figure 11: Regions of rays for $M_{h_S} = 120$ GeV, $M_{D_A} = 110$ GeV, $M_{D_{\pm}} = 110$ GeV. M_{D_H} varies.

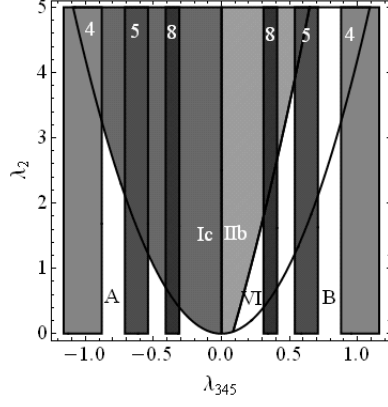


Figure 12: $(\lambda_{345}, \lambda_2)$ plot for low DM mass region with the WMAP-allowed areas for $M_{DH} = (8, 5, 4)$ GeV, respectively.

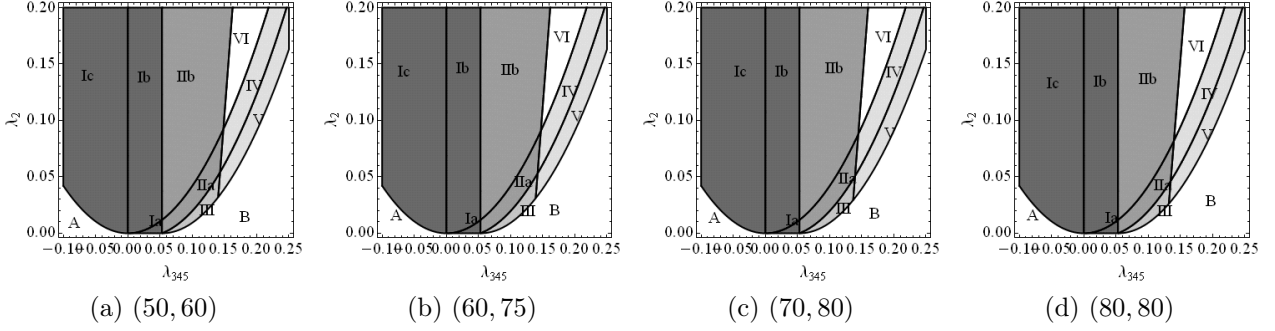


Figure 13: $M_{DH} = 40$ GeV, $M_{h_S} = 120$ GeV. M_{DA} and $M_{D\pm}$ vary. Cases (a-d) done for the pairs (δ_A, δ_{\pm}) GeV.

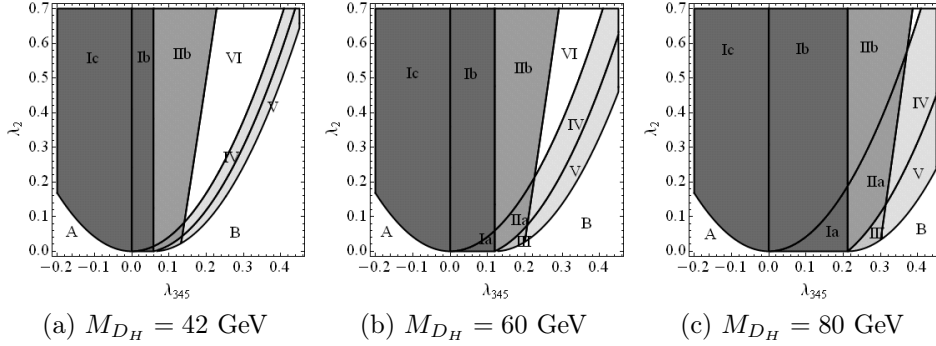


Figure 14: Medium mass region for $\delta_A = 8$ GeV, $\delta_{\pm} = 50$ GeV.

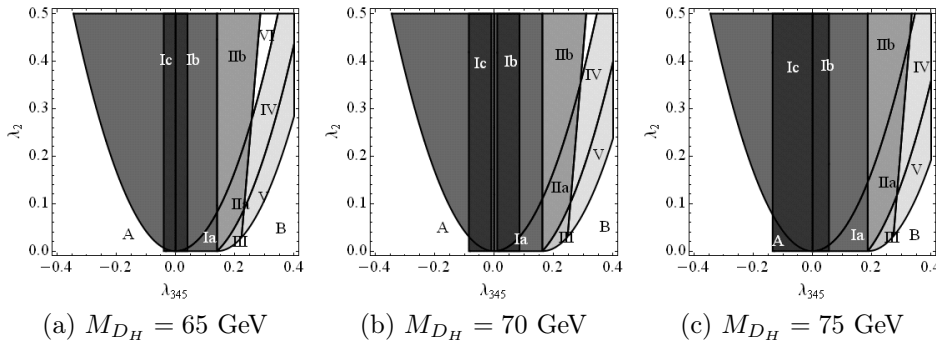


Figure 15: Medium mass region for $\delta_A = 8$ GeV, $\delta_{\pm} = 50$ GeV. Vertical dark areas correspond to the relic density in 3σ WMAP range.

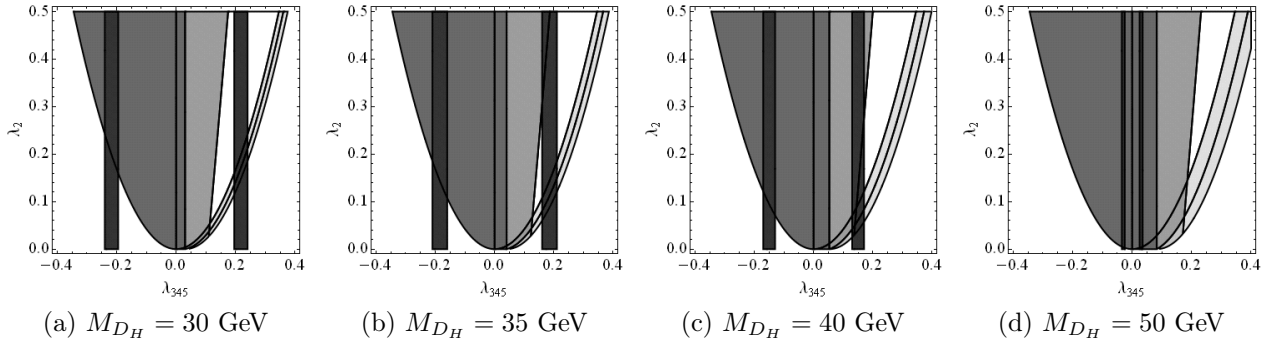


Figure 16: Medium mass region for $\delta_A = 70$ GeV, $\delta_{\pm} = 70$ GeV. Vertical dark areas correspond to the relic density in 3σ WMAP range.